

Article

# Monazite Alteration in $\text{H}_2\text{O} \pm \text{HCl} \pm \text{NaCl} \pm \text{CaCl}_2$ Fluids at 150 °C and $p_{\text{sat}}$ : Implications for Uranium Deposits

Antonin Richard \*, Jean-Marc Montel, Romain Leborgne, Chantal Peiffert, Michel Cuney and Michel Cathelineau

Received: 23 July 2015 ; Accepted: 9 October 2015 ; Published: 16 October 2015  
Academic Editor: Mostafa Fayek

GeoRessources lab., Université de Lorraine, CNRS, CREGU, Boulevard des Aiguillettes B.P. 70239, F-54506 Vandoeuvre-lès-Nancy, France; jean-marc.montel@univ-lorraine.fr (J.-M.M.); romain.leborgne@hotmail.fr (R.L.); chantal.peiffert@univ-lorraine.fr (C.P.); michel.cuney@univ-lorraine.fr (M.Cu.); michel.cathelineau@univ-lorraine.fr (M.Ca.)

\* Correspondence: antonin.richard@univ-lorraine.fr; Tel.: +33-383-684-737; Fax: +33-383-684-701

**Abstract:** Spectacular alteration of monazite by diagenetic/hydrothermal brines is well documented in some Proterozoic sedimentary basins in close relationship with high-grade uranium (U) deposits. Hence, monazite has been proposed as a viable source for some U deposits. However, monazite alteration remains enigmatic with regard to its high stability in relatively low temperature hydrothermal conditions. Here, the results of batch experiments in which 10 mg of natural monazite grains were reacted with 15 mL of Na-Ca-Cl (6 molal Cl) solutions as well as in pure water at 150 °C and saturated vapor pressure ( $p_{\text{sat}}$ ) for one and six months are reported. The influence of pH (pH = 1, 3, 7) and relative molar proportions of Na and Ca ( $\text{Na}/(\text{Na} + \text{Ca}) = 0, 0.5, 1$ ), were tested. Discrete alteration features (etch pits and roughened surfaces) appear in a minority of the one month experiments and are more developed in the six months experiments, especially at pH = 1 and 3. Although spectacular alteration of monazite, as seen around U deposits, could not be reproduced here, this study shows that monazite is unstable in the presence of fluids analogous to acidic deep basinal brines.

**Keywords:** monazite; hydrothermal; alteration; uranium; experimental

## 1. Introduction

Monazite is a Light Rare Earth Element (LREE) orthophosphate, with the formula  $(\text{LREE})\text{PO}_4$ , and a common accessory mineral in magmatic and metamorphic rocks. Monazite is known for its great capacity to integrate tetravalent actinides like U(IV) and Th(IV) [1–3]. Contrary to U- and Th-rich silicates, monazite is not affected by metamictization due to self-irradiation [4,5]. Furthermore, occurrence of detrital monazite in beach sands and sandstones shows that monazite is highly stable in most crustal and surficial conditions [6,7]. Hence, monazite has been widely used as a U-Th-Pb geochronometer [8–10] and has been considered as a confining matrix for nuclear waste storage [11–13]. However, under some specific metamorphic, hydrothermal and surficial conditions, monazite instability has been demonstrated [14–27]. As a consequence, alteration of monazite can lead to disturbances of U-Th-Pb geochronologic systems [15,28–32]. Because monazite instability may result in the release of U, Th, Pb and REE, it has been considered as a potential source mineral for some U deposits, U oxides being in turn frequently enriched in REE [17,33–38].

Spectacular alteration of monazite in the presence of deep basinal brines is well documented in some Proterozoic sedimentary basins and their crystalline basements in close relationship with

high-grade U deposits, especially in the Athabasca Basin (Canada), McArthur Basin (Australia) and Franceville Basin (Gabon) [16–18,39,40]. The aim of this work is to test experimentally the stability of monazite in the conditions that have prevailed during the formation of world-class U deposits in the Athabasca, McArthur and Franceville Basins. For this purpose, batch experiments have been carried out in which natural monazite grains were reacted with 6 molal Cl, Na-Ca-Cl brines with variable Na/(Na + Ca) molar ratios and pH at 150 °C and  $p_{\text{sat}}$  in autoclaves with one and six months run times.

## 2. Background

The geological background of the Proterozoic basins where spectacular alteration of monazite has been described, the world-class uranium deposits within those basins, the petrography of altered monazites and the fluid conditions that have prevailed during alteration of monazite are reported here.

### 2.1. Proterozoic Basins and Uranium Deposits

High-grade and large-tonnage  $\text{UO}_2$  deposits (up to 200 kt of U at 20% U on average at McArthur River deposit) are located close to the basement unconformity of the Paleoproterozoic Athabasca Basin (Saskatchewan, Canada) [41,42]. These U deposits originate from protracted basin-scale circulation of U-bearing fluids, at *ca.* 1.5–1.2 Ga, through sedimentary and basement rocks concurrent with sediment diagenesis at temperatures of 150–200 °C [43–47]. This style of “unconformity-related” uranium deposits is unique to a restricted number of Proterozoic basins including the Athabasca and Thelon Basins (Canada) [48,49] and the McArthur Basin (Northern Australia) [50–52]. Comparable processes may have been responsible for the famous Oklo U deposits in the Franceville Basin (Gabon), which on account of their high grades and greater age  $\sim$ 2 Ga formed natural nuclear reactors [46].

### 2.2. Monazite Alteration and U Sources in Proterozoic Basins and Basements

Potential sources of uranium for U deposits in those Proterozoic basins include mainly: (i) accessory minerals (apatite, zircon, monazite) in the basins and their basement [16,17,39,40,44,53] and (ii) vein-type  $\text{UO}_2$  within metamorphic rocks and magmatic  $\text{UO}_2$  within granitic pegmatites, as described in the basement rocks of the eastern margin of the Athabasca Basin [54–56].

In the sub-Athabasca basement (especially in pegmatoids and potassic orthogneisses), altered monazites are mostly found in intensively hydrothermally altered areas (illite-chlorite) [17,57]. Monazite is altered to Th-silicate (thorite or huttonite), Si-bearing Ca-Th-phosphates (cheralite, brabantite or brockite) and small euhedral grains of LREE-Sr-Ca-Fe aluminous hydroxy-phosphates (APS) of the crandallite group (Figure 1). Similarly, in the hydrothermally altered basement rocks of the McArthur Basin, altered monazites are associated with APS minerals [39,58]. In the silicified sandstones of the Franceville Basin, detrital monazite is altered to Th-silicate (huttonite or thorite) [16]. In all cases, electron microprobe analysis of unaltered and altered monazites shows that *ca.* 75% of the U initially bound to the monazite is leached.

### 2.3. Fluid Conditions for Monazite Alteration

The fluids presumed to be responsible for monazite alteration in the Athabasca, McArthur and Franceville Basins share many physical-chemical similarities, as determined mainly from fluid inclusion studies [40,44–47,50,51,59–63]. In those three basins, the fluids are *ca.* 120–200 °C high chlorinity (*ca.* 6 molal Cl), acidic (pH = 3–6), aqueous Na-Ca-Cl dominated brines with highly variable Na/(Na + Ca) molar ratios (*ca.* 0.2 to 0.8) with so-called “NaCl-rich brine” and “ $\text{CaCl}_2$ -rich brine” end-members. Pressure estimations from fluid inclusions range from *ca.* 0.5 to 1.2 kbars. Besides  $\text{Na}^+$  and  $\text{Ca}^{2+}$ , the NaCl-rich brine and  $\text{CaCl}_2$ -rich brine are also enriched in  $\text{K}^+$ ,  $\text{Mg}^{2+}$  at the  $10^3$  to  $10^4$  mg/L level. Halogen (Cl, Br, I), stable chlorine isotope composition of fluid inclusions and stable boron isotope compositions of tourmaline have shown that these brines originate from

surface evaporation of seawater [40,45,46,64–68]. These brines have undergone significant chemical modifications (e.g., Na-Ca, Na-K, Ca-Mg exchanges, U leaching) after interacting with basin and basement rocks as seen from the differences between evaporated seawater and fluid inclusions compositions [46,61,63,65].

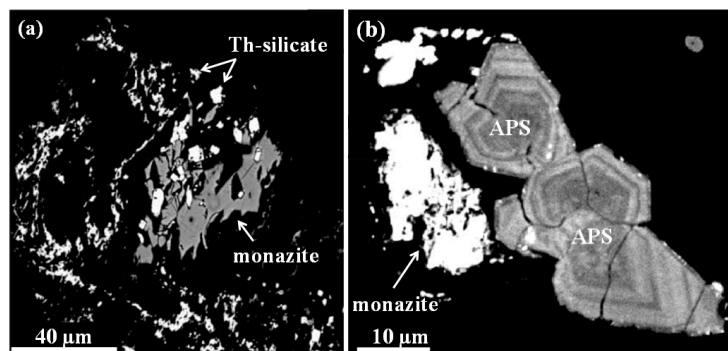


**Figure 1.** Examples of intensive alteration of monazite by diagenetic/hydrothermal brines from the basement of the Proterozoic Athabasca Basin (Canada): (a) Back-scattered electron image of a monazite grain (grey), which is nearly completely altered to Th-silicate (white) (modified from [17]). (b) Back-scattered electron image of a relict monazite (white) associated with aluminum phosphate-sulfate mineral (APS) (grey) (modified from [57]).

### 3. Experimental

The preparation of the starting material for the experiments (natural monazite from Manangotry, Madagascar), the composition of the starting material, the preparation of the experiments, the experimental conditions and the analytical conditions for scanning electron microscope analyses of monazite grains before and after the experiments, are described hereby.

#### 3.1. Scanning Electron Microscope Analyses

Secondary electron and backscattered electron imaging of monazite grains (before and after experiments) was performed using a JEOL JSM7600F scanning electron microscope (SEM) (JEOL Ltd., Tokyo, Japan) equipped with energy dispersive spectrometer (EDS) and a wavelength dispersive spectrometer (WDS) at the Service Commun de Microscopies Electroniques et de Microanalyses (SCMEM, GeoRessources lab., Nancy, France).

#### 3.2. Starting Material

A cm-size monocrystal of natural monazite from Manangotry (Madagascar) was selected as starting material for the experiments (Figure 2a) [69]. This sample is described in details in [70] (referred to as PK6). Briefly, monazite in Manangotry occurs as N 45°, 35°–40° SE monazite-apatite-biotite-garnet-zircon-quartz lodes cutting coarse grain granite. Chemical (U-Th-Pb) dating by electron microprobe of this sample yielded  $542 \pm 11$  Ma [70]. Electron microprobe analysis performed using analytical conditions similar to those described in [7] shows that this sample has a highly homogeneous composition (Table 1) [70]. Besides P and REE, this samples shows  $1.99 \pm 0.13$  (1 $\sigma$ ) wt % SiO<sub>2</sub>,  $0.95 \pm 0.08$  (1 $\sigma$ ) wt % CaO,  $0.31 \pm 0.17$  (1 $\sigma$ ) wt % PbO,  $12.93 \pm 0.75$  (1 $\sigma$ ) wt % ThO<sub>2</sub> and  $0.28 \pm 0.09$  (1 $\sigma$ ) wt % UO<sub>2</sub>. This composition is very close to that published earlier [71].

**Table 1.** Electron microprobe analysis for the starting experimental material (monazite from Manangotry, Madagascar). Average ( $n = 32$ ) composition ( $\mu$ ) and standard deviation ( $1\sigma$ ) are expressed in weight percent (wt %). Note that  $\text{Eu}_2\text{O}_3$ ,  $\text{Tb}_2\text{O}_3$ ,  $\text{Ho}_2\text{O}_3$ ,  $\text{Er}_2\text{O}_3$ ,  $\text{Tm}_2\text{O}_3$  and  $\text{Yb}_2\text{O}_3$  were not analyzed. After [70].

Concentration	$\text{SiO}_2$	$\text{P}_2\text{O}_5$	$\text{CaO}$	$\text{Y}_2\text{O}_3$	$\text{La}_2\text{O}_3$	$\text{Ce}_2\text{O}_3$	$\text{Pr}_2\text{O}_3$	$\text{Nd}_2\text{O}_3$	$\text{Sm}_2\text{O}_3$	$\text{Gd}_2\text{O}_3$	$\text{Dy}_2\text{O}_3$	$\text{PbO}$	$\text{ThO}_2$	$\text{UO}_2$	Total
$\mu$ (wt %)	1.99	26.58	0.95	0.12	13.76	28.31	2.91	9.78	1.05	0.43	0.04	0.31	12.93	0.28	99.44
$\pm 1\sigma$ (wt %)	0.13	0.30	0.08	0.07	0.41	0.48	0.35	0.39	0.28	0.27	0.08	0.17	0.75	0.09	-

### 3.3. Sample Preparation

The monazite monocrystal was first crushed in a confined hydraulic press. The crushed material was then sieved and the  $>200\ \mu\text{m}$  fraction was hand-crushed in an agate pestle and mortar. All the crushed material was sieved again and the  $60\text{--}105\ \mu\text{m}$  fraction was recovered for the experiments. The  $60\text{--}105\ \mu\text{m}$  fraction of crushed material was processed by a Franz magnetic separator in order to remove mineral impurities (plagioclase, pyroxene, apatite, and thorite). Optical examination under binoculars of the resulting  $60\text{--}105\ \mu\text{m}$  fraction revealed  $<1\%$  mineral impurities (Figure 2b). The  $60\text{--}105\ \mu\text{m}$  fraction was then rinsed twice in distilled water. Examination of crushed monazite grains by secondary electron imaging shows clean surfaces and angular grain shapes (Figure 2c). No indication of metamictization has been observed. Examination of crushed and mounted monazite grains by back-scattered electron imaging shows highly homogeneous composition (Figure 2d), as seen by electron microprobe analysis (Table 1).

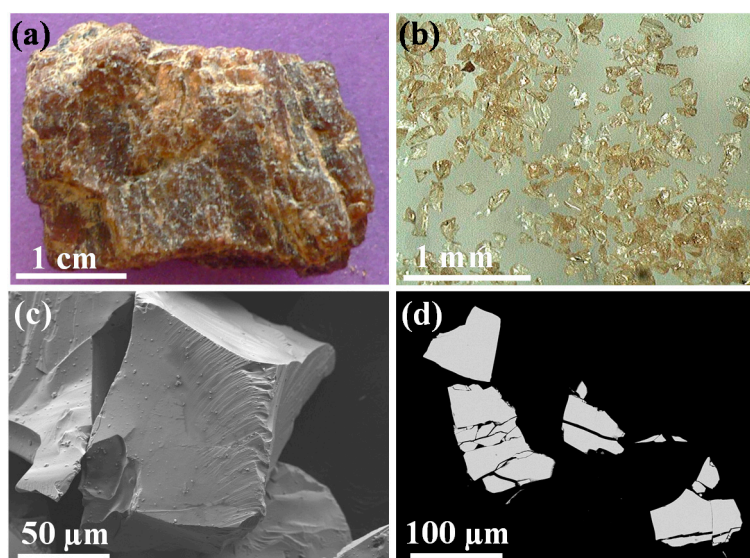


**Figure 2.** Starting experimental material: (a) Photograph of the natural monazite monocrystal from Manangotry (Madagascar) selected for this study (sample PK6 in [70]). (b) Photograph under binoculars of crushed, sieved and purified by magnetic separation,  $60\text{--}105\ \mu\text{m}$  monazite grains from the monocrystal shown in (a). (c) Secondary electron image of one of the monazite grains shown in (b). (d) Back-scattered electron image of some of the mounted monazite grains shown in (b).

### 3.4. Batch Experiments

Experimental solutions were prepared using (i) distilled water with a resistance over length of  $18.2\ \text{M}\Omega\cdot\text{cm}^{-1}$ ; (ii)  $\text{CaCl}_2\cdot 2\text{H}_2\text{O}$  PROLABO 22322.295 powder; (iii)  $\text{NaCl}$  AnalR NORMAPUR 95%–97% powder; and (iv) hydrochloric acid provided by Riedel de Haen as  $\text{HCl}\text{--}\text{H}_2\text{O}$  mixture saturated with  $\text{HCl}$  (37% by mass). A total of twelve experimental solutions were prepared. Three solutions were prepared with variable  $\text{Na}/(\text{Na} + \text{Ca})$  molar ratios of 0, 0.5 and 1. Then, from each of the three solutions with different  $\text{Na}/(\text{Na} + \text{Ca})$  values, three different solutions were prepared

with pH values of 1, 3 and 7, adjusted with HCl and a pH-meter calibrated using calibration buffer solutions. All of those nine solutions have a total Cl concentration of 6 molal. Finally, three solutions were prepared with distilled water and no salts and pH values of 1, 3 and 7, adjusted with HCl and a pH-meter. For each experiment, 10 mg of purified 60–105  $\mu\text{m}$  fraction of monazite grains were weighted in a Mettler AT 201 (Mettler-Toledo, Greifensee, Switzerland) precision balance. Monazite grains and 15 mL of experimental solutions were then placed in twelve 20 mL polytetrafluoroethylene (PTFE) containers, which were in turn placed in twelve autoclaves, and heated at 150 °C under saturated vapor pressure ( $p_{\text{sat}}$ ) in a sealed ceramic oven. After one month and six months, each autoclave was extracted, quickly cooled by water quenching, and opened.

#### 4. Results

Experimental conditions, experiment numbers and observations by SEM of monazite grains after one month and six months experiments are reported in Tables 2 and 3 respectively. Observations are reported hereafter according to experiment numbers (EXP#). SEM images of the different alteration features on monazite grains are shown in Figures 3 and 4 for one month and six months experiments respectively.

**Table 2.** Experimental conditions, experiment numbers (#) and observations by SEM of monazite grains after one month experiments.

Experiment #	Cl (molal)	Na/(Na + Ca)	pH	Observations
EXP# 1	6	0	1	no alteration
EXP# 2	6	0	3	no alteration
EXP# 3	6	0	7	no alteration
EXP# 4	6	0.5	1	etch pits and roughened surfaces
EXP# 5	6	0.5	3	etch pits
EXP# 6	6	0.5	7	no alteration
EXP# 7	6	1	1	etch pits and roughened surfaces
EXP# 8	6	1	3	no alteration
EXP# 9	6	1	7	no alteration
EXP# 10	H <sub>2</sub> O + HCl		1	no alteration
EXP# 11	H <sub>2</sub> O + HCl		3	no alteration
EXP# 12	H <sub>2</sub> O		7	no alteration

**Table 3.** Experimental conditions, experiment numbers and observations by SEM of monazite grains after six months experiments.

Experiment #	Cl (molal)	Na/(Na + Ca)	pH	Observations
EXP# 13	6	0	1	etch pits and roughened surfaces
EXP# 14	6	0	3	no alteration
EXP# 15	6	0	7	no alteration
EXP# 16	6	0.5	1	etch pits and roughened surfaces
EXP# 17	6	0.5	3	roughened surfaces
EXP# 18	6	0.5	7	no alteration
EXP# 19	6	1	1	etch pits and roughened surfaces
EXP# 20	6	1	3	etch pits
EXP# 21	6	1	7	no alteration
EXP# 22	H <sub>2</sub> O + HCl		1	etch pits and roughened surfaces
EXP# 23	H <sub>2</sub> O + HCl		3	no alteration
EXP# 24	H <sub>2</sub> O		7	no alteration

#### 4.1. One Month Experiments

One month experiments with pure H<sub>2</sub>O and H<sub>2</sub>O-HCl mixtures (pH = 1, 3, 7) (EXP# 10, 11, 12) show no alteration of the surface of monazite grains. Experiments with NaCl and/or CaCl<sub>2</sub> show contrasting results. EXP# 1, 2, 3, 6, 8, 9 show no alteration of the surface of monazite grains. All experiments at pH = 7 (EXP# 3, 6, 9, 12) and experiments with CaCl<sub>2</sub> only (EXP# 1, 2, 3) show no alteration of the surface of monazite grains. Only EXP# 4, 5 and 7 show some etch pits (Figure 3a,b) and/or roughened surfaces (Figure 3c,d). Note that those alteration features were not systematically observed on all grain surfaces for a given experiment. This could be due to the fact that some surfaces were not or very little exposed to the experimental solutions at places where grains were close to each other.

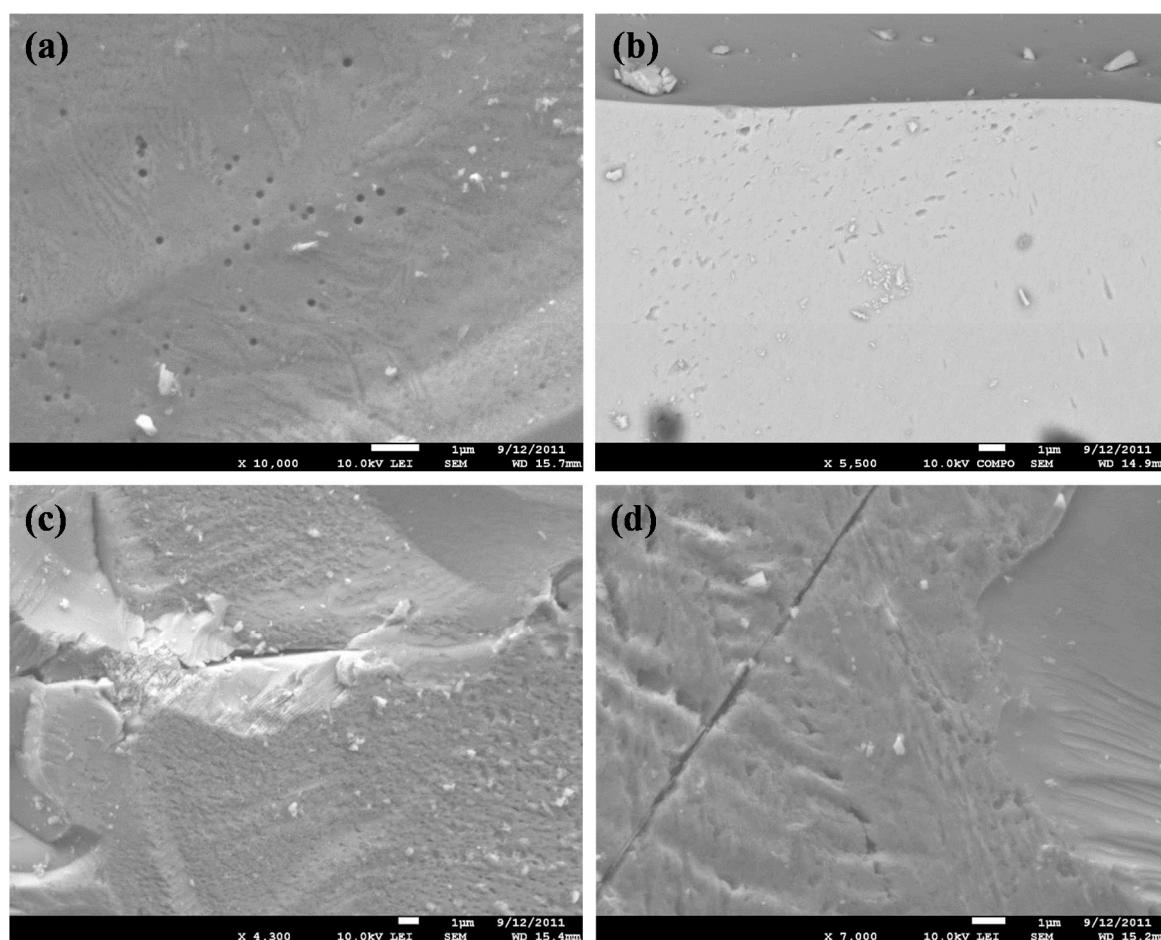


**Figure 3.** SEM images of the different alteration features on monazite grains after one month experiments: (a) etch pits in EXP# 7; (b) etch pits in EXP# 5; and (c,d) roughened surfaces in EXP# 4.

#### 4.2. Six Months Experiments

Six months experiments show significantly more developed alteration features compared to the one month experiments, although not widespread. Types of alteration features are similar to those in one month experiments and consist of etch pits and roughened surfaces. Etch pits seem to develop first, leading to roughened surfaces when the pit density is high (Figure 4a–e). Similarly to one month experiments, alteration features were not systematically observed on all grain surfaces for a given experiment, possibly due to the fact that some surfaces were not or very little exposed to the experimental solutions at places where grains were close to each other. Etch pits and roughened surfaces are systematically visible in experiments at pH = 1 (EXP# 13, 16, 19, 22).

All experiments at pH = 7 (EXP# 15, 18, 21, 24) show no alteration of the surface of monazite grains. The most intensively altered monazite grains form in EXP# 17 where roughened surfaces are well developed (Figure 4e). Roughened surfaces appear to be heterogeneous in composition; however their small-scale compositional variability does not permit further investigation (Figure 4f).

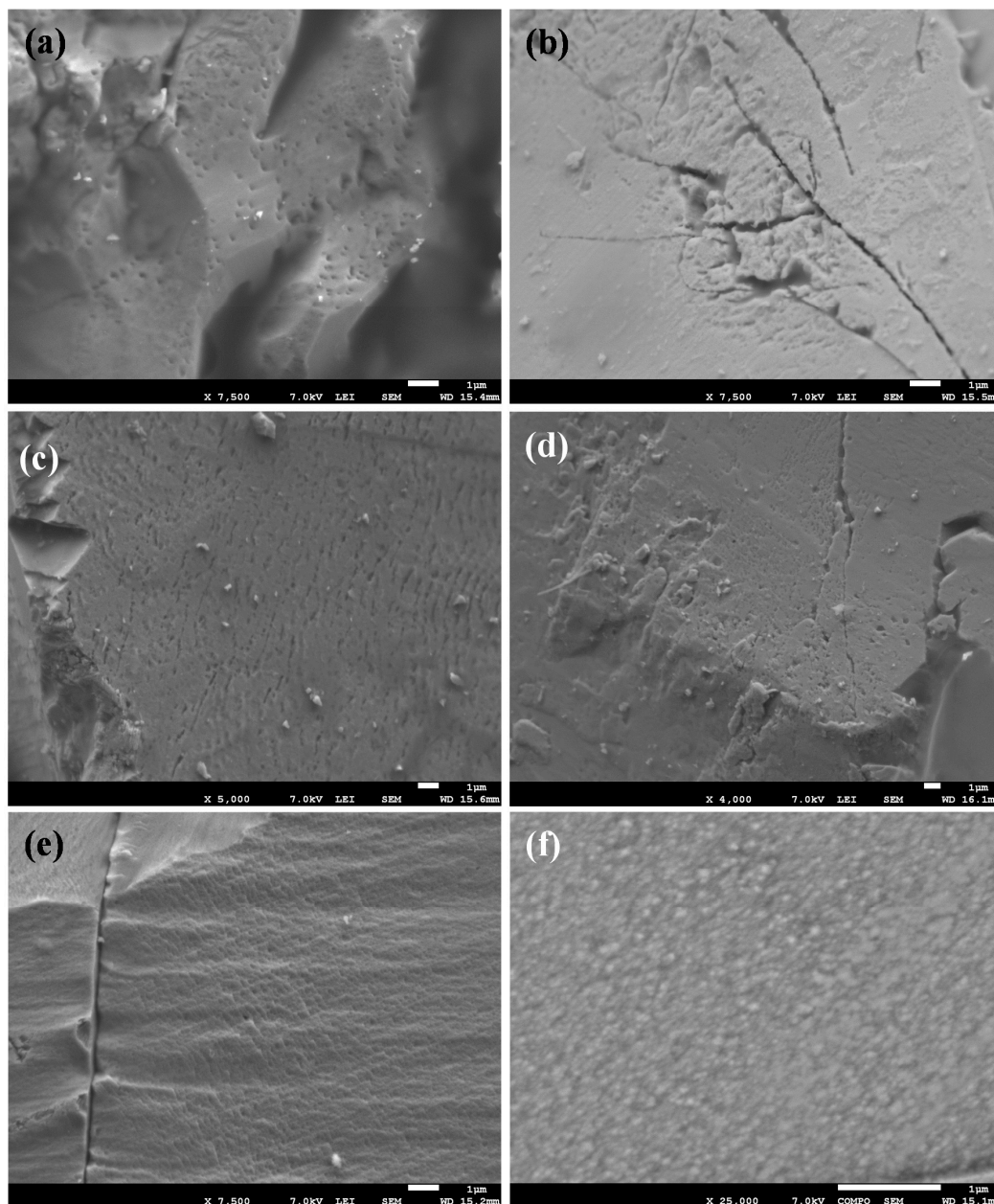


**Figure 4.** SEM images of the different alteration features on monazite grains after the six months experiments: (a) etch pits in EXP# 20; (b) etch pits and roughened surface in EXP# 13; (c) etch pits and roughened surface in EXP# 22; (d) etch pits and roughened surface in EXP# 16; (e) roughened surface in EXP# 17; and (f) zoom into roughened surface in EXP# 17.

## 5. Discussion

The influence of the different experimental parameters and the implications of the experiments results on monazite stability in  $\text{H}_2\text{O} \pm \text{HCl} \pm \text{NaCl} \pm \text{CaCl}_2$  fluids at 150 °C and  $p_{\text{sat}}$  for uranium deposits, are discussed here.

### 5.1. Significance of Alteration Features

Etch pits observed here look similar to those observed for experiments involving brines at 500 °C and 500 MPa [24] and dissolution pits, grooves and patterns observed for experiments in H<sub>2</sub>O-NaCl at 800 °C [72]. The etch pits and roughened surfaces show some morphological similarities with “leached surfaces” observed for experiments in aqueous solutions at 100–250 °C and  $p_{\text{sat}}$  [73] and dissolution near ledge features observed for experiments in 20–230 °C acidic aqueous solutions [71].

Therefore, etch pits combined with the absence of residual crystals on grain surfaces may indicate congruent monazite dissolution. Conversely, the heterogeneous nature of roughened surfaces (Figure 4f) is more indicative of fluid-mediated dissolution-reprecipitation.

### 5.2. Influence of Starting Material

The experimental setup used here is very simple and does not include additional minerals besides monazite. Minerals unstable in those conditions could promote alteration of monazite by supplying ions necessary to form secondary phases as observed in nature like Si, Al or S to form APS and Th-silicates. From the few published experiments at relatively low temperature, monazite replacement by REE-rich steacyite under P-T conditions of 250–350 °C and 200–400 MPa, with starting materials including monazite + albite + K-feldspar + muscovite + biotite + SiO<sub>2</sub> + CaF<sub>2</sub> and Na<sub>2</sub>Si<sub>2</sub>O<sub>5</sub> + H<sub>2</sub>O has been demonstrated [32]. Similarly, experiments involving monazite + albite ± K-feldspar + muscovite ± biotite + SiO<sub>2</sub> + CaF<sub>2</sub> and a variety of fluids, at 450 to 500 °C and 450 to 610 MPa, showed alteration of monazite to allanite, REE-epidote, fluorapatite, and/or fluorapatite-britholite [24]. Further experiments using for example granitic powder in order to mimic the mineralogical environment of monazite in the basement of the Athabasca and McArthur Basins could help to better approaching natural conditions for monazite alteration in U deposits from Proterozoic basins.

### 5.3. Influence of Temperature and Pressure

One possible limiting factor explaining that alteration of monazite as seen in Proterozoic basins could not be reproduced in the present experiments could be the relatively low temperature of 150 °C. Although temperature may have evolved during the lifespan of the hydrothermal systems in the Proterozoic Athabasca, McArthur and Franceville Basins, with various estimates ranging from 100 to 250 °C [40,45,50,63], most fluid inclusion data point to 150 °C as a reasonably good representative temperature for the NaCl-rich and CaCl<sub>2</sub>-rich brines. Monazite alteration and uranium mobilization by Na-Ca-Cl brines at temperature >500 °C have been demonstrated in some uranium deposits in the Western Zambian Copperbelt [74,75]. Even though such high temperature is unlikely to have been reached in the Athabasca, McArthur and Franceville Basins, it cannot be excluded that relatively short high temperature events, significantly hotter than the average temperature of 150 °C, have occurred and could be associated with monazite alteration events. Factors such as fluid density and dynamic viscosity will be significantly affected by the pressure prevailing during the experiments. Here,  $p_{\text{sat}}$  is well below the pressure of *ca.* 0.5 to 1.2 kbars at the base of the Proterozoic Basins [40,45,50,63]. However, from the current knowledge on monazite solubility, the influence of pressure on monazite alteration in the present experimental conditions is hardly predictable [76].

### 5.4. Influence of Experiment Duration

Although the six month experiments do not show intense alteration of monazite, they produced significantly more alteration features than the one month experiments. This shows that monazite destabilization in those conditions is possible but is kinetically probably a very slow process. The duration of the hydrothermal systems for the formation of the Proterozoic uranium deposits in the Athabasca, McArthur and Franceville Basins is poorly constrained but various estimates are in the order of 0.1–100 Myr years [47,77,78]. It is therefore clear that experimental conditions applied

here can hardly approach the duration of those hydrothermal systems. The total amount of monazite dissolved in the present experiments is hard to constrain, most probably below 0.1%, possibly in the order of 0.001% to 0.01%. If between 0.001% and 0.01% of the monazite is dissolved in the six months experiments, it would theoretically take  $5 \times 10^3$  to  $5 \times 10^4$  years to dissolve all 10 mg of monazite at a constant rate. Therefore, complete destabilization of monazite may have required protracted fluid flow. However, the duration for complete destabilization of monazite was probably below the lower estimate for the duration of the hydrothermal systems at the origin of uranium deposits in Proterozoic basins.

### 5.5. Influence of Fluid/Rock Ratio

With 10 mg of monazite grains and 15 mL of experimental solutions, the mass fluid/rock ratio in the experiments is  $1.5 \times 10^3$ . This is relatively high for a usual hydrothermal system but below the fluid/rock ratios of  $>10^4$  calculated after chemical mass balance for some breccia systems associated to uranium deposits in the Athabasca Basin [79]. Intense alteration of monazite in the uranium deposits in the Proterozoic basins is therefore a possible consequence of those exceptionally high fluid/rock ratios which, according to the fluid flow velocity estimates in those environments [77], agrees with durations of the hydrothermal systems in the order of 0.1–100 Myr years. Further experiments with, for instance, 1 mg of monazite grains could help test this hypothesis. However, in nature, the fluids were mobile and not static and equilibrium between the solid and the fluid was probably not achieved, which makes comparison of fluid/rock ratios between nature and the present static experiments difficult.

### 5.6. Influence of pH and Fluid Composition

The experimental results show a clear influence of pH in the destabilization of monazite, with increasing abundance of alteration features from pH = 7 to pH = 1. This is consistent with the acidic nature of the brines in the Athabasca Basin, which is also a prerequisite for efficient uranium transport [47]. Experiments in pure water with variable pH show no alteration features except for pH = 1 during six months experiments. Therefore, pH and not the ionic strength of the brines, is the dominant control on monazite alteration under these conditions. The Na/(Na + Ca) ratio appears to have also some control on monazite destabilization with increasing abundance of alteration features from Na/(Na + Ca) values of 0 to 1 and then 0.5. CaCl<sub>2</sub>-rich brines have been shown to carry *ca.* one order of magnitude more uranium than NaCl-rich brines in the Athabasca Basin [61,63]. If monazite is effectively the main uranium source in those brines, this could mean that brines with a low Na/(Na + Ca) ratio would be more aggressive with respect to monazite. This would also be consistent with the observed formation of Ca-Th phosphates and Ca-bearing aluminum phosphate-sulfate minerals as a product of monazite destabilization in the Athabasca Basin [17]. However, this hypothesis cannot be confirmed by the present results. Instead, the results indicate that mix-salt solutions are the most efficient for monazite destabilization. This requires a mixing of the NaCl-rich and CaCl<sub>2</sub>-rich brine end-members prior to destabilizing the monazite. It is noteworthy that the alteration features are best developed for pH = 3 and a Na/(Na + Ca) ratio of 0.5 in the six months experiments. Those conditions appear to be the closest to the natural conditions where pH is thought to be between 3 and 4, and brine mixing is widespread [45–47,61,63]. Finally, further experiments could be carried out with fluid composition approaching more closely the compositions of the NaCl-rich and CaCl<sub>2</sub>-rich brines, as determined for the Athabasca Basin by [61,63]. Indeed, the composition of the NaCl-rich and CaCl<sub>2</sub>-rich brines in the Athabasca Basin, with notably high Mg<sup>2+</sup> and K<sup>+</sup> content besides Na<sup>+</sup> and Ca<sup>2+</sup>, is fairly unusual compared to more usual diagenetic brines largely dominated by Na-Ca-Cl [80]. Further experiments with KCl and MgCl<sub>2</sub>-rich brines and mixed-salt brines could help better understanding the competing roles of cations for monazite destabilization in those solutions and possibly better constrain which of the so-called “NaCl-rich

brine” or “CaCl<sub>2</sub>-rich brine” or their mixing terms is responsible for the spectacular alteration of monazite in U deposits in Proterozoic basins.

## 6. Conclusions

Taken together, batch experiments using 10 mg of natural monazite grains and 15 mL of acidic to neutral Na-Ca-Cl (6 molal Cl) brines at 150 °C and  $p_{\text{sat}}$  for one month and six months show limited alteration of the monazite grains. Some discrete alteration features (etch pits and roughened surfaces) have developed, especially in acidic solution, indicating that natural monazite is unstable in these conditions, but alteration is very slow. This contrasts with spectacular alteration of monazite in analogous natural conditions observed in the Proterozoic Athabasca, McArthur and Franceville Basins where monazite is partially to fully replaced by Th-silicates and aluminum phosphate-sulfate (APS) minerals. Spectacular alterations observed in nature may therefore have required more protracted fluid/rock interaction, higher fluid/rock ratios or unusual brine composition. Further experiments involving additional reactive minerals together with monazite (e.g., granite powder) could also provide more favorable conditions for monazite alteration, closer to natural conditions.

**Acknowledgments:** This work was supported by a ICEEL-CARNOT postdoctoral grant to A.R. and a CNRS-GUTEC (Géologie de l’Uranium et du Thorium, Extraction, Conversion) grant to J.M.M. The authors warmly acknowledge Anne-Magali Seydoux-Guillaume, Laurent Truche and Julien Mercadier for fruitful discussions and Sandrine Mathieu for assistance during SEM analyses. Peter Tropper and two anonymous reviewers are warmly thanked for their constructive comments as well as Mostafa Fayek and Fan Wang for editorial handling.

**Author Contributions:** A.R. performed the experiments and handled the paper, including the text and figures. R.L. greatly helped preparing the starting monazite material for the experiments. C.P. greatly helped in performing the experiments. A.R., J.M.M., M.Cu. and M.Ca. raised funds, conceived the project and designed the experiments.

**Conflicts of Interest:** The authors declare no conflict of interest.

## References

1. Förster, H.J. The chemical composition of REE-Y-Th-U-rich accessory minerals in peraluminous granites of the Erzgebirge-Fichtelgebirge region, Germany, Part I: The monazite-(Ce)-brabantite solid solution series. *Am. Mineral.* **1998**, *83*, 259–272.
2. Boatner, L.A. Synthesis, structure, and properties of monazite, pretulite, and xenotime. *Rev. Mineral. Geochem.* **2002**, *48*, 87–121. [[CrossRef](#)]
3. Spear, F.S.; Pyle, J.M. Apatite, monazite and xenotime in metamorphic rocks. *Rev. Mineral. Geochem.* **2002**, *48*, 293–335. [[CrossRef](#)]
4. Meldrum, A.; Boatner, L.A.; Weber, W.J.; Ewing, R.C. Radiation damage in zircon and monazite. *Geochim. Cosmochim. Acta* **1998**, *62*, 2509–2520.
5. Seydoux-Guillaume, A.M.; Wirth, R.; Deutsch, A.; Schärer, U. Microstructure of 24–1928 Ma concordant monazites; implications for geochronology and nuclear waste deposits. *Geochim. Cosmochim. Acta* **2004**, *68*, 2517–2527. [[CrossRef](#)]
6. Roy, P.S. Heavy mineral beach placers in southeastern Australia; their nature and genesis. *Econ. Geol.* **1999**, *94*, 567–588. [[CrossRef](#)]
7. Montel, J.M.; Razafimahatratra, D.; Ralison, B.; de Parseval, P.; Thibault, M.; Randranja, R. Monazite from mountain to ocean: A case study from Trolognaro (Fort-Dauphin), Madagascar. *Eur. J. Mineral.* **2011**, *23*, 745–757. [[CrossRef](#)]
8. Parrish, R.R. U–Pb dating of monazite and its application to geological problems. *Can. J. Earth Sci.* **1990**, *27*, 1431–1450. [[CrossRef](#)]
9. Harrison, T.M.; Catlos, E.J.; Montel, J.M. U-Th-Pb dating of phosphate minerals. *Rev. Mineral. Geochem.* **2002**, *48*, 524–558. [[CrossRef](#)]
10. Catlos, E.J. Generalizations about monazite: Implications for geochronologic studies. *Am. Mineral.* **2013**, *98*, 819–832. [[CrossRef](#)]

11. Ewing, R.C.; Wang, L. Phosphates as nuclear waste forms. *Rev. Mineral. Geochem.* **2002**, *48*, 673–699. [[CrossRef](#)]
12. Montel, J.M.; Glorieux, B.; Seydoux-Guillaume, A.M.; Wirth, R. Synthesis and sintering of a monazite-brabantite solid solution ceramic for nuclear waste storage. *J. Phys. Chem. Solids* **2006**, *67*, 2489–2500. [[CrossRef](#)]
13. Dacheux, N.; Clavier, N.; Podor, R. Monazite as a promising long-term radioactive waste matrix: Benefits of high-structural flexibility and chemical durability. *Am. Mineral.* **2013**, *98*, 833–847. [[CrossRef](#)]
14. Poitrasson, F.; Chenery, S.; Bland, D.J. Contrasted monazite hydrothermal alteration mechanisms and their geochemical implications. *Earth Planet. Sci. Lett.* **1996**, *145*, 79–96. [[CrossRef](#)]
15. Poitrasson, F.; Chenery, S.; Shepherd, T.J. Electron microprobe and LA-ICP-MS study of monazite hydrothermal alteration: Implications for U-Th-Pb geochronology and nuclear ceramics. *Geochim. Cosmochim. Acta* **2000**, *64*, 3283–3297. [[CrossRef](#)]
16. Cuney, M.; Mathieu, R. Extreme light REE mobilization by diagenetic fluids in the geological environment of the Oklo natural reactor zones, Franceville basin, Gabon. *Geology* **2000**, *28*, 743–746. [[CrossRef](#)]
17. Hecht, L.; Cuney, M. Hydrothermal alteration of monazite in the Precambrian basement of the Athabasca basin: Implications for the genesis of unconformity related deposits. *Miner. Deposita* **2000**, *35*, 791–795. [[CrossRef](#)]
18. Mathieu, R.; Zetterström, L.; Cuney, M.; Gauthier-Lafaye, F.; Hidaka, H. Alteration of monazite and zircon and lead migration as geochemical tracers of fluid paleocirculations around Oklo-Okélobondo and Bangombé natural nuclear reaction zones (Gabon). *Chem. Geol.* **2001**, *171*, 147–171. [[CrossRef](#)]
19. Read, D.; Andreoli, M.A.G.; Knoper, M.; Williams, C.T.; Jarvis, N. The degradation of monazite Implications for the mobility of rare-earth and actinide elements during low-temperature alteration. *Eur. J. Mineral.* **2002**, *14*, 487–498. [[CrossRef](#)]
20. Harlov, D.E.; Wirth, R.; Hetherington, C.J. The relative stability of monazite and huttonite at 300–900 °C and 200–1000 MPa: Metasomatism and the propagation of metastable mineral phases. *Am. Mineral.* **2007**, *92*, 1652–1664. [[CrossRef](#)]
21. Harlov, D.E.; Wirth, R.; Hetherington, C.J. Fluid-mediated partial alteration in monazite: The role of coupled dissolution–reprecipitation in element redistribution and mass transfer. *Contrib. Mineral. Petr.* **2011**, *162*, 329–348. [[CrossRef](#)]
22. Rasmussen, B.; Muhling, J.R. Reactions destroying detrital monazite in greenschist-facies sandstones from the Witwatersrand basin, South Africa. *Chem. Geol.* **2009**, *264*, 311–327. [[CrossRef](#)]
23. Budzyń, B.; Hetherington, C.J.; Williams, M.L.; Jercinovic, M.J.; Michalik, M. Fluid–mineral interactions and constraints on monazite alteration during metamorphism. *Mineral. Mag.* **2010**, *74*, 659–681. [[CrossRef](#)]
24. Budzyń, B.; Harlov, D.E.; Williams, M.L.; Jercinovic, M.J. Experimental determination of stability relations between monazite, fluorapatite, allanite, and REE-epidote as a function of pressure, temperature, and fluid composition. *Am. Mineral.* **2011**, *96*, 1547–1567. [[CrossRef](#)]
25. Hetherington, C.J.; Harlov, D.E.; Budzyń, B. Experimental metasomatism of monazite and xenotime: Mineral stability, REE mobility and fluid composition. *Miner. Petrol.* **2010**, *99*, 165–184. [[CrossRef](#)]
26. Harlov, D.E.; Hetherington, C.J. Partial high-grade alteration of monazite using alkali-bearing fluids: Experiment and nature. *Am. Mineral.* **2010**, *95*, 1105–1108. [[CrossRef](#)]
27. Seydoux-Guillaume, A.M.; Montel, J.M.; Bingen, B.; Bosse, V.; de Parseval, P.; Paquette, J.L.; Janots, E.; Wirth, R. Low-temperature alteration of monazite: Fluid mediated coupled dissolution–precipitation, irradiation damage, and disturbance of the U–Pb and Th–Pb chronometers. *Chem. Geol.* **2012**, *330*, 140–158. [[CrossRef](#)]
28. Seydoux-Guillaume, A.M.; Paquette, J.L.; Wiedenbeck, M.; Montel, J.M.; Heinrich, W. Experimental resetting of the U-Th-Pb systems in monazite. *Chem. Geol.* **2002**, *191*, 165–181. [[CrossRef](#)]
29. Bosse, V.; Boulvais, P.; Gautier, P.; Tiepolo, M.; Ruffet, G.; Devidal, J.L.; Cherneva, Z.; Gerdjikov, I.; Paquette, J.L. Fluid-induced disturbance of the monazite Th-Pb chronometer: *In situ* dating and element mapping in pegmatites from the Rhodope (Greece, Bulgaria). *Chem. Geol.* **2009**, *261*, 286–302. [[CrossRef](#)]
30. Williams, M.L.; Jercinovic, M.J.; Harlov, D.E.; Budzyń, B.; Hetherington, C.J. Resetting monazite ages during fluid-related alteration. *Chem. Geol.* **2011**, *283*, 218–225. [[CrossRef](#)]

31. Didier, A.; Bosse, V.; Boulvais, P.; Bouloton, J.; Paquette, J.L.; Montel, J.M.; Devidal, J.L. Disturbance *versus* preservation of U–Th–Pb ages in monazite during fluid–rock interaction: Textural, chemical and isotopic *in situ* study in microgranites (Velay Dome, France). *Contrib. Mineral. Petr.* **2013**, *165*, 1051–1072. [[CrossRef](#)]
32. Budzyń, B.; Konečný, P.; Kozub-Budzyń, G.A. Stability of monazite and disturbance of the Th–U–Pb system under experimental conditions of 250–350 °C and 200–400 MPa. *Ann. Soc. Geol. Pol.* **2015**, *85*, 405–424. [[CrossRef](#)]
33. Pagel, M. The mineralogy and geochemistry of uranium, thorium, and rare-earth elements in two radioactive granites of the Vosges, France. *Mineral. Mag.* **1982**, *46*, 151–163. [[CrossRef](#)]
34. Negga, H.S.; Sheppard, S.M.F.; Rosenbaum, J.; Cuney, M. Late Hercynian U-vein mineralization in the Alps: Fluid-inclusions and C, O, H isotopic evidence for mixing between two externally derived fluids. *Contrib. Mineral. Petr.* **1986**, *90*, 52–62. [[CrossRef](#)]
35. Pagel, M.; Pinte, G.; Rotach-Toulhoat, N. The rare earth elements in natural uranium oxides. *Monogr. Ser. Miner. Depos.* **1987**, *27*, 81–85.
36. Cathelineau, M. Accessory mineral alteration in peraluminous granites at the hydrothermal stage: A review. *Rendiconti-Societa Italiana di Mineralogia e Petrologia* **1988**, *43*, 499–507.
37. Cathelineau, M.; Poty, B. U-Th-REE mobility in granitic environments at the hydrothermal stage. In *Metallogenesis of Uranium Deposits*; International Atomic Energy Agency: Vienna, Austria, 1989; pp. 63–77.
38. Mercadier, J.; Cuney, M.; Lach, P.; Boiron, M.C.; Bonhoure, J.; Richard, A.; Leisen, M.; Kister, P. Origin of uranium deposits revealed by their rare earth element signature. *Terra Nova* **2011**, *23*, 264–269. [[CrossRef](#)]
39. Cuney, M.; Brouand, M.; Hecht, L.; Bruneton, P. Contrasted Rare Earth mobility during hydrothermal alteration in the Jabiluka uranium deposit (Alligator Rivers district, Northern Territory, Australia). In Proceedings of the GAC-MAC Annual Meeting, Calgary, AB, Canada, 29 May–1 June 2000.
40. Mathieu, R.; Cuney, M.; Cathelineau, M. Geochemistry of paleofluids circulation in the Franceville basin and around Oklo natural reaction zones (Gabon). *J. Geochem. Explor.* **2000**, *69–70*, 245–249. [[CrossRef](#)]
41. Jefferson, C.W.; Thomas, D.J.; Gandhi, S.S.; Ramaekers, P.; Delaney, G.; Brisbin, D.; Cutts, C.; Portella, P.; Olson, R.A. Unconformity associated uranium deposits of the Athabasca Basin, Saskatchewan and Alberta. *Geol. Surv. Can. Bull.* **2007**, *588*, 23–67.
42. Kyser, T.K.; Cuney, M. Unconformity-related uranium deposits. In *Recent and Not-So-Recent Developments in Uranium Deposits and Implications for Exploration*; Cuney, M., Kyser, K., Eds.; Mineralogical Association of Canada Short Course Series: Quebec, QC, Canada, 2008; Volume 39, pp. 161–219.
43. Hoeve, J.; Sibbald, T.I.I. On the genesis of the Rabbit Lake and other unconformity-type uranium deposits in Northern Saskatchewan, Canada. *Econ. Geol.* **1978**, *73*, 1450–1473. [[CrossRef](#)]
44. Kotzer, T.G.; Kyser, T.K. Petrogenesis of the Proterozoic Athabasca Basin, Northern Saskatchewan, Canada, and its relation to diagenesis, hydrothermal uranium mineralization and paleohydrogeology. *Chem. Geol.* **1995**, *120*, 45–89. [[CrossRef](#)]
45. Derome, D.; Cathelineau, M.; Cuney, M.; Fabre, C.; Lhomme, T. Mixing of sodic and calcic brines and uranium deposition at McArthur River, Saskatchewan, Canada: A Raman and laser-induced breakdown spectroscopic study of fluid inclusions. *Econ. Geol.* **2005**, *100*, 1529–1545. [[CrossRef](#)]
46. Boiron, M.C.; Cathelineau, M.; Richard, A. Fluid flows and metal deposition near basement/cover unconformity: Lessons and analogies from Pb–Zn–F–Ba systems for the understanding of Proterozoic U deposits. *Geofluids* **2010**, *10*, 270–292. [[CrossRef](#)]
47. Richard, A.; Rozsypal, C.; Mercadier, J.; Banks, D.A.; Cuney, M.; Boiron, M.C.; Cathelineau, M. Giant uranium deposits formed from exceptionally uranium-rich acidic brines. *Nat. Geosci.* **2012**, *5*, 142–146. [[CrossRef](#)]
48. Renac, C.; Kyser, T.K.; Durocher, K.; Dreaver, G.; O'Connor, T. Comparison of diagenetic fluids in the Proterozoic Thelon and Athabasca Basins, Canada: Implications for protracted fluid histories in stable intracratonic basins. *Can. J. Earth Sci.* **2002**, *39*, 113–132. [[CrossRef](#)]
49. Beyer, S.R.; Hiatt, E.E.; Kyser, K.; Dalrymple, R.W.; Pettman, C. Hydrogeology, sequence stratigraphy and diagenesis in the Paleoproterozoic western Thelon Basin: Influences on unconformity-related uranium mineralization. *Precambrian Res.* **2011**, *187*, 293–312. [[CrossRef](#)]

50. Derome, D.; Cuney, M.; Cathelineau, M.; Dubessy, J.; Bruneton, P. A detailed fluid inclusion study in silicified breccias from the Kombolgie sandstones (Northern Territory, Australia): Application to the genesis of Middle-Proterozoic unconformity-type uranium deposits. *J. Geochem. Explor.* **2003**, *80*, 259–275. [[CrossRef](#)]
51. Derome, D.; Cathelineau, M.; Fabre, C.; Boiron, M.C.; Banks, D.A.; Lhomme, T.; Cuney, M. Paleo-fluid composition determined from individual fluid inclusions by Raman and LIBS: Application to mid-Proterozoic evaporitic Na–Ca brines (Alligator Rivers Uranium Field, northern territories Australia). *Chem. Geol.* **2007**, *237*, 240–254. [[CrossRef](#)]
52. Polito, P.A.; Kyser, T.K.; Alexandre, P.; Hiatt, E.E.; Stanley, C.R. Advances in understanding the Kombolgie Subgroup and unconformity-related uranium deposits in the Alligator Rivers Uranium Field and how to explore for them using litho-geochemical principles. *Aust. J. Earth Sci.* **2011**, *58*, 453–474. [[CrossRef](#)]
53. Fayek, M.; Kyser, T.K. Characterization of multiple fluid-flow events and rare-earth-element mobility associated with formation of unconformity-type uranium deposits in the Athabasca Basin, Saskatchewan. *Can. Mineral.* **1997**, *35*, 627–658.
54. Parslow, G.R.; Thomas, D.J. Uranium occurrences in the Cree Lake zone, Saskatchewan, Canada. *Mineral. Mag.* **1982**, *46*, 165–173. [[CrossRef](#)]
55. McKechnie, C.L.; Annesley, I.R.; Ansdell, K.M. Radioactive abyssal granitic pegmatites and leucogranites in the Wollaston Domain, northern Saskatchewan, Canada: Mineral compositions and conditions of emplacement in the Fraser Lakes area. *Can. Mineral.* **2012**, *50*, 1637–1667. [[CrossRef](#)]
56. Mercadier, J.; Annesley, I.R.; McKechnie, C.L.; Bogdan, T.S.; Creighton, S. Magmatic and metamorphic uraninite mineralization in the western margin of the Trans-Hudson Orogen (Saskatchewan, Canada): A uranium source for unconformity-related uranium deposits? *Econ. Geol.* **2013**, *108*, 1037–1065. [[CrossRef](#)]
57. Gaboreau, S.; Cuney, M.; Quirt, D.; Beaufort, D.; Patrier, P.; Mathieu, R. Aluminium phosphate sulfate minerals associated with Proterozoic unconformity-type deposits in the Athabasca Basin, Canada. *Am. Mineral.* **2007**, *92*, 267–280. [[CrossRef](#)]
58. Gaboreau, S.; Beaufort, D.; Vieillard, P.; Patrier, P.; Bruneton, P. Aluminum phosphate–sulfate minerals associated with Proterozoic unconformity-type uranium deposits in the East Alligator River Uranium Field, Northern Territories, Australia. *Can. Mineral.* **2005**, *43*, 813–827. [[CrossRef](#)]
59. Pagel, M. Détermination des conditions physico-chimiques de la silicification diagénétique des grès Athabasca (Canada) au moyen des inclusions fluides. *CR. Acad. Sci. Paris* **1975**, *280*, 2301–2304. (In French)
60. Mercadier, J.; Richard, A.; Boiron, M.C.; Cathelineau, M.; Cuney, M. Brine migration in the basement rocks of the Athabasca Basin through microfracture networks (P-Patch U deposit, Canada). *Lithos* **2010**, *115*, 121–136. [[CrossRef](#)]
61. Richard, A.; Pettke, T.; Cathelineau, M.; Boiron, M.C.; Mercadier, J.; Cuney, M.; Derome, D. Brine-rock interaction in the Athabasca basement (McArthur River U deposit, Canada): Consequences for fluid chemistry and uranium uptake. *Terra Nova* **2010**, *22*, 303–308. [[CrossRef](#)]
62. Richard, A.; Cauzid, J.; Cathelineau, M.; Boiron, M.C.; Mercadier, J.; Cuney, M. Synchrotron-XRF and XANES investigation of uranium speciation and element distribution in fluid inclusions from unconformity-related uranium deposits. *Geofluids* **2013**, *13*, 101–111. [[CrossRef](#)]
63. Richard, A.; Cathelineau, M.; Boiron, M.C.; Mercadier, J.; Banks, D.A.; Cuney, M. Metal-rich fluid inclusions provide new insights into unconformity-related U deposits (Athabasca Basin and Basement, Canada). *Miner. Deposita* **2015**, in press. [[CrossRef](#)]
64. Richard, A.; Banks, D.A.; Mercadier, J.; Boiron, M.C.; Cuney, M.; Cathelineau, M. An evaporated seawater origin for the ore-forming brines in unconformity-related uranium deposits (Athabasca Basin, Canada): Cl/Br and  $\delta^{37}\text{Cl}$  study of fluid inclusions. *Geochim. Cosmochim. Acta* **2011**, *75*, 2792–2810. [[CrossRef](#)]
65. Richard, A.; Boulvais, P.; Mercadier, J.; Boiron, M.C.; Cathelineau, M.; Cuney, M.; France-Lanord, C. From evaporated seawater to uranium-mineralizing brines: Isotopic and trace element study of quartz–dolomite veins in the Athabasca system. *Geochim. Cosmochim. Acta* **2013**, *113*, 38–59. [[CrossRef](#)]
66. Richard, A.; Kendrick, M.A.; Cathelineau, M. Noble gases (Ar, Kr, Xe) and halogens (Cl, Br, I) in fluid inclusions from the Athabasca Basin (Canada): Implications for unconformity-related U deposits. *Precambrian Res.* **2014**, *247*, 110–125. [[CrossRef](#)]

67. Leisen, M.; Boiron, M.C.; Richard, A.; Dubessy, J. Determination of Cl and Br concentrations in individual fluid inclusions by combining microthermometry and LA-ICPMS analysis: Implications for the origin of salinity in crustal fluids. *Chem. Geol.* **2012**, *330*, 197–206. [[CrossRef](#)]
68. Mercadier, J.; Richard, A.; Cathelineau, M. Boron- and magnesium-rich marine brines at the origin of giant unconformity-related uranium deposits:  $\delta^{11}\text{B}$  evidence from Mg-tourmalines. *Geology* **2012**, *40*, 231–234. [[CrossRef](#)]
69. De la Roche, H. Les indices de monazite du col de Manangotry. Etude d'ensemble provisoire. *Arch. Serv. Géol. Madagasikara* **1956**, A1082. (In French)
70. Razafimahatratra, D. La Monazite des Chaînes Anosyennes: Des Gisements en Place aux Sables de Plages à Ilménite-Zircon-Monazite. Ph.D. Thesis, Université d'Antananarivo, Antananarivo, Madagascar, 2008. (In French)
71. Oelkers, E.H.; Poitrasson, F. An experimental study of the dissolution stoichiometry and rates of a natural monazite as a function of temperature from 50 to 230 °C and pH from 1.5 to 10. *Chem. Geol.* **2002**, *191*, 73–87. [[CrossRef](#)]
72. Tropper, P.; Manning, C.E.; Harlov, D.E. Solubility of  $\text{CePO}_4$  monazite and  $\text{YPO}_4$  xenotime in  $\text{H}_2\text{O}$  and  $\text{H}_2\text{O-NaCl}$  at 800 °C and 1 GPa: Implications for REE and Y transport during high-grade metamorphism. *Chem. Geol.* **2011**, *282*, 58–66. [[CrossRef](#)]
73. Gysi, A.P.; Williams-Jones, A.E.; Harlov, D. The solubility of xenotime-(Y) and other HREE phosphates ( $\text{DyPO}_4$ ,  $\text{ErPO}_4$  and  $\text{YbPO}_4$ ) in aqueous solutions from 100 to 250° C and  $p_{\text{sat}}$ . *Chem. Geol.* **2015**, *401*, 83–95. [[CrossRef](#)]
74. Eglinger, A.; Tarantola, A.; Durand, C.; Ferraina, C.; Vanderhaeghe, O.; André-Mayer, A.S.; Paquette, J.L.; Deloule, E. Uranium mobilization by fluids associated with Ca–Na metasomatism: A P–T–t record of fluid–rock interactions during Pan-African metamorphism (Western Zambian Copperbelt). *Chem. Geol.* **2014**, *386*, 218–237. [[CrossRef](#)]
75. Eglinger, A.; Ferraina, C.; Tarantola, A.; André-Mayer, A.S.; Vanderhaeghe, O.; Boiron, M.C.; Dubessy, J.; Richard, A.; Brouand, M. Hypersaline fluids generated by high-grade metamorphism of evaporites: Fluid inclusion study of uranium occurrences in the Western Zambian Copperbelt. *Contrib. Mineral. Petr.* **2014**, *167*. [[CrossRef](#)]
76. Pourtier, E.; Devidal, J.L.; Gibert, F. Solubility measurements of synthetic neodymium monazite as a function of temperature at 2kbars, and aqueous neodymium speciation in equilibrium with monazite. *Geochim. Cosmochim. Acta* **2010**, *74*, 1872–1891. [[CrossRef](#)]
77. Raffensperger, J.P.; Garven, G. The formation of unconformity-type uranium ore deposits 2. Coupled hydrochemical modeling. *Am. J. Sci.* **1995**, *295*, 639–696. [[CrossRef](#)]
78. Dargent, M.; Truche, L.; Dubessy, J.; Bessaque, G.; Marmier, H. Reduction kinetics of aqueous U (VI) in acidic chloride brines to uraninite by methane, hydrogen or C-graphite under hydrothermal conditions: Implications for the genesis of unconformity-related uranium ore deposits. *Geochim. Cosmochim. Acta* **2015**, *167*, 11–26. [[CrossRef](#)]
79. Lorilleux, G.; Cuney, M.; Jébrak, M.; Rippert, J.C.; Portella, P. Chemical brecciation processes in the Sue unconformity-type uranium deposits, Eastern Athabasca Basin (Canada). *J. Geochem. Explor.* **2003**, *80*, 241–258. [[CrossRef](#)]
80. Davisson, M.L.; Criss, R.E. Na-Ca-Cl relations in basinal fluids. *Geochim. Cosmochim. Acta* **1996**, *60*, 2743–2752. [[CrossRef](#)]



© 2015 by the authors; licensee MDPI, Basel, Switzerland. This article is an open access article distributed under the terms and conditions of the Creative Commons Attribution (CC-BY) license (<http://creativecommons.org/licenses/by/4.0/>).